

Development and Assessment of Pressure-Based and Model-Based Techniques for the MFB50 Control of a Euro VI 3.0L Diesel Engine

*Original*

Development and Assessment of Pressure-Based and Model-Based Techniques for the MFB50 Control of a Euro VI 3.0L Diesel Engine / Finesso, Roberto; Marelli, Omar; Misul, DANIELA ANNA; Spessa, Ezio; Violante, Massimo; Yang, Yixin; Hardy, Gilles; Maier, Christian. - In: SAE INTERNATIONAL JOURNAL OF ENGINES. - ISSN 1946-3944. - ELETTRONICO. - 10:4(2017), pp. 1538-1555. [10.4271/2017-01-0794]

*Availability:*

This version is available at: 11583/2688842 since: 2021-04-01T11:01:43Z

*Publisher:*

SAE International

*Published*

DOI:10.4271/2017-01-0794

*Terms of use:*

This article is made available under terms and conditions as specified in the corresponding bibliographic description in the repository

*Publisher copyright*

(Article begins on next page)

# Development and assessment of pressure-based and model-based techniques for the MFB50 control of a Euro VI 3.0L diesel engine

Roberto Finesso, Omar Mareello, Daniela Misul, Ezio Spessa, Massimo Violante, and Yixin Yang  
Politecnico di Torino

Gilles Hardy and Christian Maier  
FPT Motorenforschung AG

## Abstract

Pressure-based and model-based techniques for the control of MFB50 (crank angle at which 50% of the fuel mass fraction has burned) have been developed, assessed and tested by means of rapid prototyping (RP) on a FPT F1C 3.0L Euro VI diesel engine.

The pressure-based technique requires the utilization of a pressure transducer for each cylinder. The transducers are used to perform the instantaneous measurement of the in-cylinder pressure, in order to derive its corresponding burned mass fraction and the actual value of MFB50. It essentially consists of a closed-loop approach, which is based on a cycle-by-cycle and cylinder-to-cylinder correction of the start of injection of the main pulse ( $SOI_{main}$ ), in order to achieve the desired target of MFB50 for each cylinder.

The model-based technique, instead, requires the adoption of a heat release predictive model to simulate MFB50; this model is based on an improved version of the accumulated fuel mass approach, which requires the injection rate as input. This control technique is essentially based on the inversion of the heat release model, in order to identify the optimal value of  $SOI_{main}$  that allows the desired MFB50 target to be achieved cycle-by-cycle. The approach is therefore of the open-loop type.

Both control techniques were developed and assessed by means of Model-in-the-Loop (MiL) and Hardware-in-the-Loop (HiL) techniques, and then tested on the engine using a rapid prototyping device. The experimental tests were performed on a highly dynamic test bench at the Politecnico di Torino.

These techniques have shown a good potential for MFB50 control, compared to the standard methodology implemented in the Engine Control Unit (ECU).

## Introduction

The increasing computational performance of modern engine control units (ECUs) is offering the opportunity to develop and implement more and more complex techniques for combustion control in diesel engines. These techniques can lead to a significant contribution in order to reduce fuel consumption, combustion noise and engine-out emissions in real time. In this context, the control of combustion

phasing can play a significant role. One of the most frequently used combustion metrics for such types of controls is represented by MFB50, i.e., the crank angle at which 50% of the fuel mass fraction has burned. The control techniques for MFB50 control can roughly be divided into two types: closed-loop and feed-forward (or model-based) categories.

In closed-loop methods, MFB50 is diagnosed by the ECU in real-time, and is compared with a target value, which is appropriately identified in order to minimize engine-out emissions, combustion noise and fuel consumption. The injection parameters (typically, the start of injection of the main pulse) are adjusted in real-time, cycle-by-cycle, in order to achieve the desired MFB50 target [1].

In these kinds of methodologies, the MFB50 estimation is usually performed on the basis of the heat release rate that is derived from the measured in-cylinder pressure [1-4]. If each cylinder is instrumented, a cylinder-to-cylinder correction of MFB50 can also be achieved. This approach can be effective in reducing the cyclic and cylinder dispersion of MFB50, especially for highly premixed combustion modes in which high EGR levels are adopted [5], with a consequent deterioration in the combustion quality.

An alternative approach to diagnose MFB50, on the basis of the engine speed measurement, has been presented in [6-8]. This method has the advantage of not requiring any additional cost, because it is based on the instantaneous engine speed measurement that is already performed in modern engine control systems [8].

A model-based (also termed as “feed-forward”) approach, instead, is a methodology that allows MFB50 to be predicted in advance by means of a model, and which can therefore be used to adapt the main engine parameters in real-time in order to achieve the required MFB50 target. The predictive estimation of MFB50 is generally obtained by using semi-empirical methods [9] or predictive heat release rate (HRR) models [10-27]. Several approaches have been presented in the literature to simulate HRR in diesel engines.

The most detailed approach to predict the in-cylinder combustion process is represented by 3D-CFD models [10, 11]. These models have the potential of reproducing the physical and chemical processes that take place in the chamber during the injection-combustion process, but they require a considerable computational time and

suffer from the drawback of still being conditioned by a lack of precise knowledge on the physics of some processes.

Quasi-D and multizone modeling approaches [12-14] generally include a fuel spray model that is coupled with a thermodynamic combustion model. The latter is generally based on the discretization of the in-cylinder content into several homogeneous zones, to which the energy and mass conservation equations are applied. These models are capable of estimating the in-cylinder gradients of temperature and chemical composition, therefore they are suitable to be coupled with pollutant formation submodels (NO<sub>x</sub>, soot). However, they require a computational time that is not compatible with real-time combustion control applications, at least considering the computational performance of modern ECUs.

Wiebe functions [15, 16] are adopted extensively to reproduce the heat release shape, and require very little computational effort. However, the Wiebe function approach is a pure mathematical method, lacking physical consistency, because it does not link the injection rate directly to the heat release process.

Models based on the apparent combustion time have been proposed in [17, 18]. These models take into account the effects of in-cylinder air density, oxygen concentration, nozzle diameter and injection rate on the heat release rate, but do not link the injection rate with the heat release trend directly.

Models based on the accumulated fuel mass approach assume that the rate of released chemical energy is proportional to the energy associated with the fuel quantity made available for combustion at the considered moment [19-27]. This energy can be computed as the difference between the chemical energy associated with the injected fuel quantity and the cumulative heat release. This approach has the great advantage of being able to correlate the injection rate directly to the combustion process, and is therefore physically consistent. Moreover, it does not require a high calibration effort, and is therefore suitable for control-oriented applications.

Finally, the last category of models, which is often used in the field of engine design and control, includes artificial intelligence systems such as support vector machines (SVM), genetic algorithms (GA) and artificial neural networks (ANNs). These methods have been used extensively in the automotive field [28-38]. In general, they can also be referred to as “black box” or “gray box” approaches, as they do not require any detailed physical knowledge of the investigated process and are able to capture complex nonlinear system behavior by means of relatively simple mathematical operations. Moreover, they are characterized by a limited computational time, and as a result they are the best candidates for implementation in ECUs for control-oriented tasks. However, in order to be trained, they usually require a high number of experimental tests, and they are not reliable outside the pre-fixed calibration range.

### ***Contribution of the present study***

Considering the previous background, the present study has been devoted to the development of closed-loop and model-based open-loop techniques for the control of MFB50, and to their testing on a FPT F1C 3.0L Euro VI diesel engine. The closed-loop technique is based on the measurement of the in-cylinder pressure in each cylinder, and it has therefore been referred to as “pressure-based” throughout the paper.

Both control techniques were developed and assessed by means of Model-in-the-Loop (MiL) and Hardware-in-the-Loop (HiL) methods, and then tested on the engine using a rapid prototyping (RP) device. The experimental tests were performed on a highly dynamic test bench at the Politecnico di Torino.

The activity was carried out in the frame of a research project in collaboration with CNH/FPT Industrial, which is currently ongoing and which is focused on the investigation of the potential of the PCCI (Premixed Combustion Compression Ignition) combustion mode for a 3.0L diesel engine for light-duty applications. This combustion mode is in fact characterized by the use of high EGR rates in conjunction with early injection, which could lead to a significant deterioration in combustion quality, especially in transient conditions. Therefore, the implementation of a combustion control algorithms is highly recommended to guarantee stable engine operations.

However, the results reported in the present study mainly refer to the development and preliminary testing of the controls on the engine in conventional combustion mode, while the results obtained in PCCI combustion mode will be presented in the near future.

In general, the developed pressure-based technique is capable of achieving a cycle-by-cycle and cylinder-to-cylinder MFB50 control, by modulating the start of injection of the main pulse (SOI<sub>main</sub>).

The model-based technique, instead, exploits a low-throughput heat release predictive model that had previously been developed by the authors in [25] and refined in [26], which is based on an improved version of the accumulated fuel mass approach. The latter approach was selected because it has the great advantage of being able to correlate the injection rate directly to the heat release process, and is therefore physically consistent. Moreover, it is also characterized by a very fast computational time [26], which makes it possible to implement it on a rapid prototyping device for real-time cycle-by-cycle MFB50 prediction and control.

## **Engine and experimental setup**

The experimental calibration and validation tests of the developed methods were conducted on a 3.0L Euro VI diesel engine. The main technical specifications of the engine are reported in Table 1.

Table 1. Main technical specifications of the engine.

Engine type	FPT F1C Euro VI diesel engine
Displacement	2998 cm <sup>3</sup>
Bore x stroke	95.8 mm x 104 mm
Rod length	160 mm
Compression ratio	17.5
Valves per cylinder	4
Turbocharger	VGT type
Fuel injection system	High pressure Common Rail

The engine (Fig. 1) is equipped with a short-route cooled EGR system, in which the EGR valve is located upstream from the cooler. A flap is installed in the exhaust pipe downstream the turbine, to control the temperature of the exhaust gas flowing to the aftertreatment system and to allow high EGR rates to be obtained

when the pressure drop between the exhaust and intake manifolds is not sufficiently high.

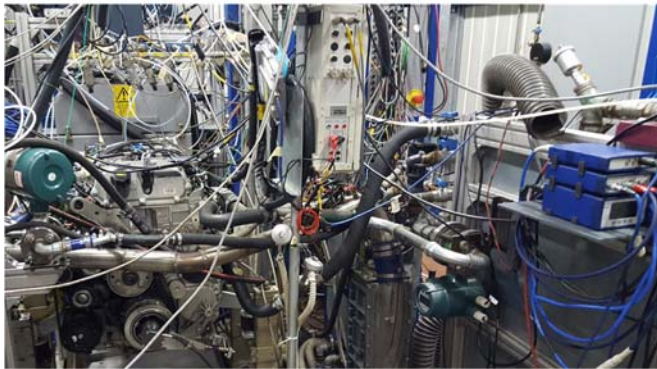


Figure 1. FPT FIC 3.0L Euro VI diesel engine installed on the highly dynamic test bench at the Politecnico di Torino. The rapid prototyping device can be observed on the right.

The test engine was instrumented with piezoresistive pressure transducers and thermocouples to measure the pressure and temperature at different locations, such as upstream and downstream from the compressor, from the turbine and intercooler, in the intake manifold and in the EGR circuit. Thermocouples were also used to measure the temperatures in each intake and exhaust runners. KISTLER 6058A high-frequency piezoelectric transducers were fitted to the glow-plug seat to measure the in-cylinder pressure time-histories, which were used for the pressure-based MFB50 control. The in-cylinder pressure traces were corrected on the basis of the intake pressure that was measured by means of high-frequency KISTLER 4007C piezoresistive transducers, which were located at the inlet runners of the cylinders.

All the experimental tests were carried out on the highly dynamic test bed at ICEAL at the Politecnico di Torino. The test rig is equipped with an ‘ELIN AVL APA 100’ cradle mounted AC dynamometer and an ‘AVL KMA 4000’, with a reading accuracy of 0.1% over a 0.28-110 kg/h range, to continuously measure the fuel consumption. An ‘AVL AMAi60’ system, consisting of three analyzer trains, was used to measure the engine-out gaseous raw emissions. Two analyzer trains were equipped with complete devices for the analysis of THC, CH4, NOx, and low as well as high CO, CO2 and O2, and were used to measure the intake and exhaust gas composition. All of the abovementioned measurement devices were controlled by a PUMA OPEN 1.3.2 automation system. In order to minimize the testing effort, the test bed environment was interfaced with AVL CAMEO software to run intelligent engine calibration procedures on the basis of the DoE (Design of Experiment) approach.

### Rapid prototyping device and real-time engine emulator

An ETAS ES910 rapid prototyping device was used to test the developed controls on the engine. This device is in fact capable of by-passing the standard functionalities of the ECU. For this purpose, the novel control algorithm was modeled using Simulink and deployed on the ETAS ES910 hardware using ETAS Intecrio software tool.

The main specifications of the ETAS ES910 device are reported in Tab. 2.

Table 2. Main specifications of the ETAS ES910 rapid prototyping device.

Main processor	Freescale PowerQUICC™ III MPC8548 with 800 MHz clock Double precision floating point unit
Memory	512 MByte DDR2-RAM (400 MHz clock) 64 MByte Flash 128 kByte NVRAM
ECU and bus interfaces	ETK 1 Channel, ETK Mode: Basic, Compatibility, Advanced ETK bypass method: hook based or service based (Service Based Bypass (SBB V2) and SBB V3) XETK / iLinkRT™ 1 channel, bypass in parallel to measurement and calibration possible iLinkRT™ connection to test bench for INCA-MCE CAN 2 Channels, High Speed (up to 1 MBaud) or Low Speed LIN 2 Channels, LIN V2.0 Extension modules ES920.1 FlexRay Module (1 Node) or ES921.1 CAN Module (2 Channels) EtherCAT connection to test bench for INCA-MCE

For safety reasons, the functionalities of the developed controls were preliminary tested with Hardware-in-the-Loop (HiL) testing by coupling the ETAS RP device to a real-time engine emulator. The engine emulator was realized by means of an NI PXIe-8135 device, equipped with a 2-port CAN Interface for communication with the ETAS RP device. A real-time mean-value GT-power engine model was used to simulate engine performance with the PXI. The main specifications of the PXI device are reported in Tab. 3.

Table 3. Main specifications of the PXI device used for HiL testing.

PXI type	NI PXIe-8135
Controller	Core i7-3610QE 2.3 GHz Controller, Win 7 (64-bit)
I/O interfaces	2-port CAN Interface, High-Speed/FD
Real-time operating system	Pharlap OS
Execution mechanism	Veristand Engine
Engine model	Real-time mean-value GT-power model

### Experimental activity

The experimental tests that have been considered in the present paper include steady-state tests and transient tests, which were carried out in conventional combustion mode. The steady-state tests were mainly used to calibrate the low-throughput heat release model that was used in the model-based MFB50 control technique. To this aim, the following tests were considered (Fig. 2):

- A full engine map with baseline operating parameters.
- EGR-sweep tests at fixed key-points.

The developed control techniques were tested on the engine over different load/speed ramps and over a WHTC interval. Details on these tests are reported in the “Results and discussion” section.

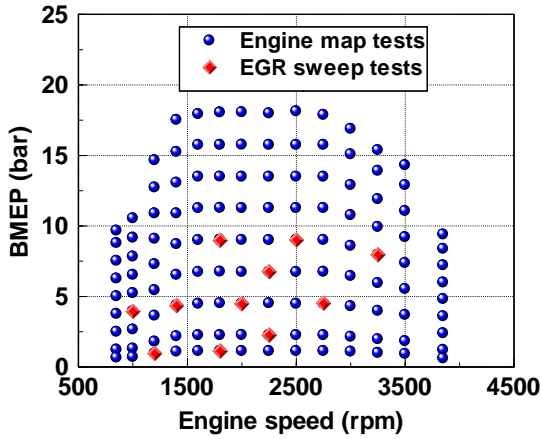


Figure 2. Experimental tests used for the calibration of the low-throughput heat release model.

## MFB50 control

### Pressure-based technique

The pressure-based technique for the control of MFB50 exploits the measurement of the in-cylinder pressure in the combustion chamber of each cylinder. In short, an MFB50 target (i.e.,  $MFB50_{tgt}$ ) is identified at a given time instant. The actual MFB50 value is extracted from the measured in-cylinder pressure of each cylinder at each cycle, and the start of injection of the main pulse (i.e.,  $SOI_{main}$ ) is then adjusted in the subsequent cycle in order to achieve the MFB50 target, according to a closed-loop approach.

In other words, the actual MFB50 value is derived from the net energy release  $Q_{net}$ , which in turn is estimated from the measured in-cylinder pressure on the basis of a single-zone approach [39], as follows:

$$dQ_{net} = \frac{\gamma}{\gamma-1} p dV + \frac{1}{\gamma-1} V dp \quad (1)$$

where  $\gamma = \frac{c_p}{c_v} = 1.37$ ,  $p$  is the measured in-cylinder pressure and  $V$  is

the in-cylinder volume. It should be noted that, in general,  $\gamma$  depends on the composition of the burned gas (see [25]) and has a significant impact on the heat release shape obtained from a single-zone heat release approach. However, it was decided to use a constant value of  $\gamma$  in order to reduce the computational time. A value of 1.37 has been set in order to be coherent with the outcomes of the acquisition software installed at the test bench, which implements the abovementioned value of  $\gamma$ .

The net energy release curve is then normalized to its maximum value in order to estimate the burned mass fraction curve, and MFB50 is obtained as the crank angle at which the normalized heat release curve is equal to 0.5. The MFB50 correction algorithm is described hereafter.

The actual MFB50 value for the generic cylinder 'j' and cycle 'i', i.e.,  $MFB50_i^j$ , is compared with the target value, i.e.,  $MFB50_{tgt,i}^j$ . The

error between the target and the actual values of MFB50 is then estimated as follows:

$$Err_i^j = MFB50_{tgt,i}^j - MFB50_i^j \quad (2)$$

The start of injection of the main pulse in the subsequent cycle, 'i+1', is corrected according to the following equation:

$$SOI_{main,i+1}^j = SOI_{main,i}^j + K_{m,i}^j \cdot Err_i^j \quad (3)$$

where  $K_{m,i}^j$  is a modulation factor that was introduced in order to optimize the response of the controller and to guarantee stable operations.

It was in fact verified that the behavior of the control can be unstable if the value of  $K_{m,i}^j$  is set constant and equal to 1 (see the "Results and discussion" section), and it is therefore necessary to adjust its value cycle-by-cycle.

An optimal strategy for the definition of the  $K_{m,i}^j$  parameter was identified during the Model-in-the-Loop (MiL) phase, in order to guarantee a fast response of the controller and to avoid the occurrence of instability. In particular, the value of  $K_{m,i}^j$  was limited to the [0.1-1] range, and was varied, cycle-by-cycle, as a function of the sign of the error between two consecutive cycles, according to the following method:

$$\begin{aligned} K_{m,i}^j &\in [0.1, 1] \\ \text{if } \text{sign}(Err_i^j) &= \text{sign}(Err_{i-1}^j): K_{m,i}^j = K_{m,i-1}^j \cdot 2 \\ \text{if } \text{sign}(Err_i^j) &\neq \text{sign}(Err_{i-1}^j): K_{m,i}^j = \frac{K_{m,i-1}^j}{2} \\ \text{if } Err_i^j &\geq 3: K_{m,i}^j = 1 \end{aligned} \quad (4)$$

The boundary values of  $K_{m,i}^j$  were identified on the basis of simulations carried out in the MiL phase. In particular, this range has been found to provide a good response time of the control without any instability issue. The initial value has been set at 0.5.

### Model-based technique

The model-based technique implements a predictive heat release model that is based on an improved version of the accumulated fuel mass approach [26], and is therefore of the open-loop type. The control has been realized by means of a model inversion. The combustion model is in fact able to simulate the heat release and MFB50 for a given set of injection parameters. The inverted model receives the MFB50 target as input, and identifies the  $SOI_{main}$  value that allows the desired target to be achieved by means of an iterative procedure.

The energy release was simulated by adopting an enhanced version [26] of the baseline model presented by the authors in [25], which is based on the accumulated fuel mass approach.

The accumulated fuel mass approach assumes that the rate of chemical energy released by the fuel, at any time instant  $t$ , is proportional to the energy associated with the in-cylinder accumulated fuel mass. This energy, at time instant  $t$ , is the difference between the chemical energy of the injected fuel mass and the released chemical energy.

It was verified in [26] that this approach leads to accurate results for pilot injections. For this reason, the chemical energy release rate was evaluated as follows:

$$\frac{dQ_{ch,pil,j}}{dt}(t) = K_{pil,j} [Q_{fuel,pil,j}(t - \tau_{pil,j}) - Q_{ch,pil,j}(t)] \quad (5)$$

where  $K_{pil,j}$  and  $\tau_{pil,j}$  are model calibration quantities related to the combustion rate and to the ignition delay, respectively, and  $Q_{fuel,pil,j}$  is the chemical energy associated with the injected fuel mass. It should be noted that the fuel evaporation process is not modeled by the accumulated fuel mass approach, therefore, the  $Q_{fuel}$  term refers to the energy associated with the globally injected fuel mass, independently on its actual phase.

The chemical energy release of the main pulse was instead simulated by means of a modified formulation that had been proposed in [26]:

$$\begin{aligned} \frac{dQ_{ch,main}}{dt}(t) &= K_{1,main} [Q_{fuel,main}(t - \tau_{main}) - Q_{ch,main}(t)] \\ &+ K_{2,main} \frac{dQ_{fuel,main}(t - \tau_{main})}{dt} \end{aligned} \quad (6)$$

The formulation proposed in Eq. (6) needs an additional calibration parameter to the Eq. (5) baseline approach (i.e.,  $K_{2,main}$ ).

From a physical point of view, the term that is proportional to the injection rate takes into account the effect of the turbulence induced by the fuel injection on the heat release, which is not negligible in diesel sprays.

The chemical energy  $Q_{fuel}$  associated to the injected fuel quantity is defined for each injection pulse  $j$  as follows:

$$Q_{fuel,j}(t) = \int_{t_{SOI,j}}^t \dot{m}_{f,inj}(t) H_L dt \quad t \leq t_{EOI,j} \quad (7)$$

$$Q_{fuel,j}(t) = \int_{t_{SOI,j}}^{t_{EOI,j}} \dot{m}_{f,inj}(t) H_L dt \quad t > t_{EOI,j} \quad (8)$$

where  $t_{SOI}$  is the start of the injection time,  $t_{EOI}$  is the end of the injection time,  $H_L$  is the lower heating value of the fuel and  $\dot{m}_{f,inj}$  is the fuel mass injection rate. The approach therefore requires the injection rate as input. A triangular injection rate, which is calculated on the basis of the injection parameters (injection timings/quantities and injection pressure), has been used, taking into account the nozzle opening delay (NOD) and nozzle closure delays (NCD) of the injector, which are obtained from look-up tables as a function of the energizing time and injection pressure.

The total chemical energy release is given by the sum of the contributions of all the injection pulses:

$$Q_{ch} = \sum_{j=1}^n Q_{ch,j} \quad (9)$$

It can be noted, from Eqs. (1-2), that the baseline approach described in [25] was used for the pilot shots, as it had already been verified that it provides satisfactory results [26].

Instead, an enhanced formulation, which includes an additional term proportional to the injection rate, was developed for the main pulse. It had been verified in [26] that the addition of this term leads to an increase in the accuracy of the predicted heat release trend and of MFB50, especially for high-load operating conditions, where the combustion of the main pulse is of the premixed/mixing-controlled type.

In general, it can be noted that the model takes into account the effects of variations in the injection rate or duration on the heat release rate curve and therefore on MFB50, because the injection profile is a direct input to the model (see Eqs. (5-8)). This approach is therefore physically consistent.

The model was assessed considering the steady-state conditions reported in Fig. 2. In particular, the optimal  $\tau$  and  $K$  parameters were identified by comparing the predicted and experimentally-derived heat release profiles, and minimizing the sum of errors and the MFB50 prediction error by means of a genetic algorithm (see [26]). The adopted correlation variables for ignition delay were chosen in accordance with the study proposed in [40]. In particular, at the beginning, all the engine variables were included in the correlations, and a sensitivity analysis was carried out in order to exclude the least influential ones, thus a stepwise regression was adopted. This approach was also adopted to identify the engine variables that had to be included in all the correlations reported hereafter.

The following correlations were identified as functions of the in-chamber thermodynamic quantities at SOI/SOC (start of injection/start of combustion) and of other engine variables:

$$K_{pil} \left[ \frac{1}{\text{deg}} \right] = 2.49 e^{-0.05 p_f^{0.4449}} O_2^{1.38} n^{1.065} q_{pil,tot}^{-0.293} \quad (10)$$

$$K_{1,main} \left[ \frac{1}{\text{deg}} \right] = 0.0059 \rho_{SOC,main}^{0.608} O_2^{0.761} n^{-0.159} q_{main}^{-0.243} \quad (11)$$

$$K_{2,main} [-] = 2.34 p_f^{0.369} \rho_{SOC,main}^{-0.847} O_2^{-0.016} n^{-0.404} q_{main}^{0.299} \quad (12)$$

$$\tau_{pil} [\text{deg}] = 15.61 p_f^{0.659} \rho_{SOIP}^{-1.97} \quad (13)$$

$$\tau_{main} [\text{deg}] = 24.57 p_f^{-1.43} \rho_{SOI,main}^{-2.59} n^{1.73} q_{f,inj}^{0.625} \quad (14)$$

$\rho_{SOI}$ ,  $T_{SOI}$ ,  $\rho_{SOC}$  and  $T_{SOC}$  in equations (10-14) indicate the in-chamber densities and temperatures evaluated at the start of injection or combustion, respectively, and were expressed in  $\text{kg/m}^3$  and K. They can be estimated in real-time on the basis of the intake manifold pressure and temperature [25], which are known quantities of the



ECU. The injection pressure  $p_f$  is expressed in bars, the engine speed  $n$  in rpm, the total injected fuel quantity  $q_{f,inj}$  (used as a load parameter) in  $\text{mm}^3/\text{cyc}/\text{cyl}$ , the total injected fuel quantity of the pilot shots  $q_{pil,tot}$  in  $\text{mm}^3/\text{cyc}/\text{cyl}$  and the intake oxygen concentration  $O_2$  in %. The in-chamber thermodynamic conditions evaluated at SOC were selected for the combustion rate parameters, as they were considered more representative than those evaluated at SOI. Differently from the study reported in [40], the effect of the intake  $O_2$  concentration has not been found to be significant for the prediction of the ignition delay of the main pulse. This is mainly due to the fact that the experimental tests considered in the present study were characterized by a more limited variation range of intake  $O_2$  concentration.

All the input model parameters were derived in real-time from the ECU variables, except for the  $O_2$  intake concentration. The latter quantity was estimated by means of a sub-model, which is summarized hereafter.

First, the total inducted mass  $m_{ind}$ , which is the sum of the trapped air and EGR mass, was estimated using a feed-forward neural network, which was trained on the basis of the experimental tests shown in Fig.2:

$$m_{ind} = \text{NeurNet}(N, p_{int}, T_{int}) \quad (15)$$

The trapped EGR mass was then estimated by subtracting the measured trapped air mass  $m_{air,meas}$  (which is derived from the engine MAF flow sensor) from the total inducted mass:

$$m_{EGR} = m_{ind} - m_{air,meas} \quad (16)$$

Finally, the  $O_2$  intake concentration was estimated as a function of the  $X_r/\lambda$  parameter (see [41]), where  $X_r$  is the EGR rate and  $\lambda$  is the relative air-to-fuel ratio:

$$O_2 = -20.35 \frac{X_r}{\lambda} + 20.79, \quad X_r = \frac{m_{EGR}}{m_{ind}} \quad (17)$$

## Model inversion

The physical model was inverted in order to predict the  $SOI_{main}$  value which that allows the desired MFB50 target to be reached. Model inversion is in fact mandatory if the model is to be used in a combustion control algorithm in which MFB50 is set as a target.

The model was inverted by adopting an iterative procedure, in which the first run was based on the initial assumption of the  $SOI_{main}$  control variable and a cycle-based integral control was applied to adjust the control variable value in order to attain convergence of the target variables (i.e.,  $MFB50_{tgt}$ ). The iterative procedure stops when the difference between the predicted value and required value of the target variable falls below the predefined threshold. In general, it was shown in [26] that convergence can be achieved after two or three iterations, when a reasonable threshold level is set (e.g., 0.2 degree for MFB50). The controller is able to increase or decrease its own integral gain according to the instantaneous error in order to accelerate convergence.

Figure 3 shows the model inversion scheme.

Page 6 of 18

7/20/2015

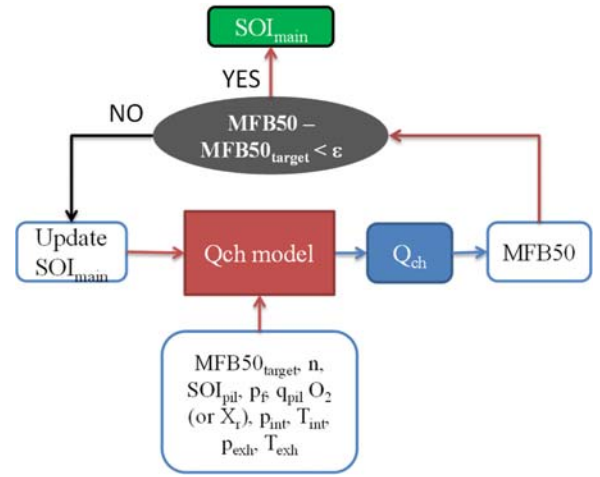


Figure 3. Flow chart of the inverted  $Q_{ch}$  model.

## Mil, HiL and RP setups

### MiL setup

The pressure-based and model-based techniques for MFB50 control were developed, assessed and tested on the engine following three steps, i.e., Model-in-the-Loop, (MiL), Hardware-in-the-Loop (HiL) and Rapid Prototyping (RP).

In the MiL phase, the control techniques were developed in Matlab/Simulink, and subsequently tested by coupling the Simulink tool to an engine emulator that was constituted by a fast-running engine model developed in GT-power. The aim of this phase was to develop, assess and test the functionality of the controls.

The tests were performed on a 2.8GHz i7 PC. The fast-running GT-power model scheme is represented in Fig.4.

The fast-running model was developed by simplifying a detailed GT-power engine model. The simplification consisted in reducing the number of pipes, in increasing the discretization length and in simplifying the EGR cooler and intercooler systems, while maintaining the same detailed simulation as the in-cylinder combustion process. A fast-running model was preferred to a detailed model in order to save computational time for HiL testing. The real-time factor of the fast-running model (i.e., the ratio between the time required for the simulation and the simulated time interval length) is of the order of 0.9, while that of the detailed model is of the order of 20. However, the accuracy of both models, especially for in-cylinder combustion process, is very similar. Details on the accuracy of the models are reported in the Appendix.

It can be seen in the figure that the model includes three controllers, i.e.:

1. A VGT controller, which acts on the turbine rack in order to reach the desired boost pressure target.
2. An EGR controller, which acts on the EGR valve diameter in order to reach the desired EGR rate target.
3. A BMEP controller, which acts on the total injected fuel mass in order to reach the desired BMEP target.

The in-cylinder combustion process was predicted by the DIPulse V73 embedded submodel.

It can be seen in the figure that a block was included in order to exchange data with the Simulink software during the MiL simulations. As far as the pressure-based technique is concerned, the Simulink tool receives the actual MFB50 values from GT-power, performs the  $SOI_{main}$  correction according to Eqs. (2-4), and sends the updated values of  $SOI_{main}$  back to GT-power. Instead, as far as the model-based technique is concerned, the Simulink tool receives the required input variables for the low-throughput heat release model from GT-power (see Fig. 3), evaluates the  $SOI_{main}$  value to reach the desired MFB50 target according to the procedure shown in Fig. 3, and sends this value back to the GT-power model.

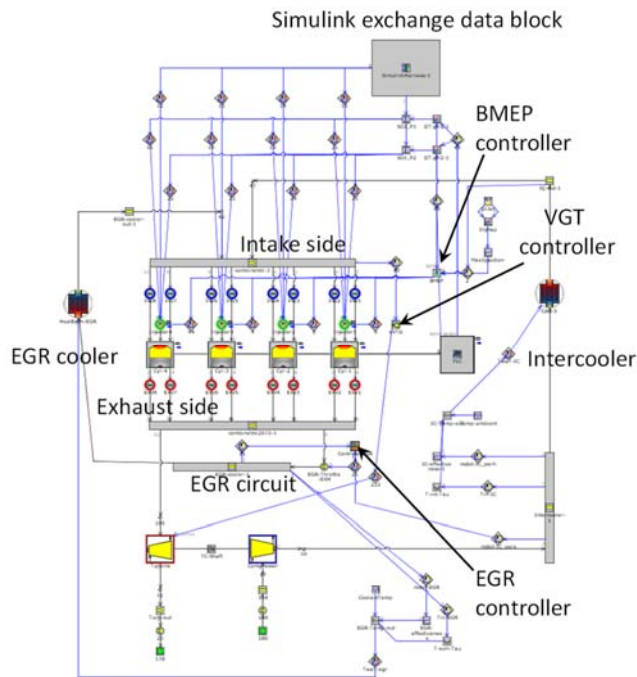


Figure 4. Scheme of the fast-running GT-power model used for MiL.

### HiL setup

In the HiL phase, the controls developed in the Simulink environment were implemented on a rapid prototyping device (i.e., ETAS ES910) through ETAS Intecrio software. The RP device was coupled to a real-time engine emulator represented by an NI PXI device equipped with a real-time engine model (see Table 3). The latter model was set up by converting the fast-running GT-power model shown in Fig. 4 into a mean-value engine model, in which the performance of the cylinders (i.e., IMEP, Exhaust temperatures, volumetric efficiency, MFB50) were estimated through feed-forward neural networks. The fast-running GT-power model could not in fact be used in real-time on the PXI because some model templates (such as the DIPulse used for heat release simulation) were not available for this mode. The communication between the PXI and the RP device was realized via CAN communication. The aim of the HiL phase was to test the computational time required by the controls when it was implemented on the RP device, as well as to test their functionalities in real-time. The HiL setup is shown in Fig. 5.

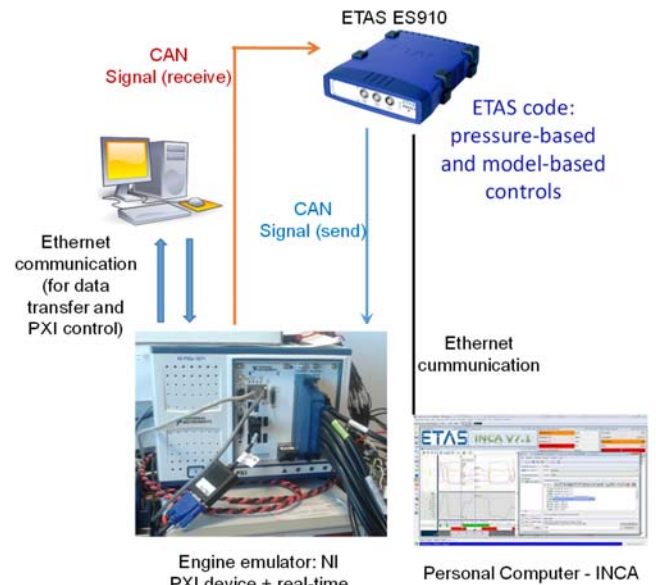


Figure 5. Scheme of the HiL setup.

### RP setup

The rapid prototyping phase had the aim of verifying the functionalities of the controls on the real engine.

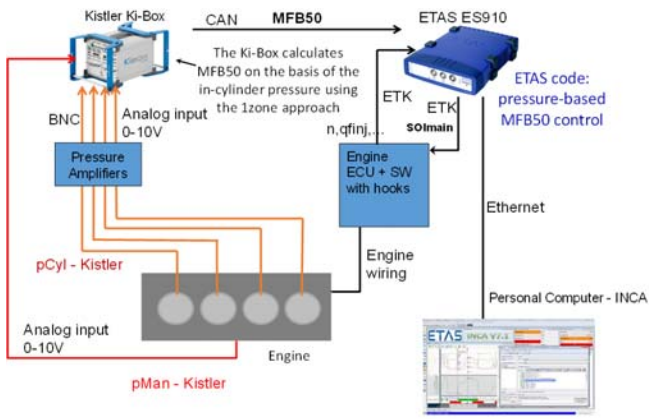
The RP setup for the pressure-based and model-based MFB50 control techniques is shown in Fig. 6a and Fig. 6b, respectively

With reference to the setup for the pressure-based technique (Fig. 6a), a Kistler Kibox was used to derive the actual MFB50 values in real-time and cycle-by-cycle from the in-cylinder pressure traces acquired in each cylinder, using a single-zone approach (i.e., Eq. (1)). The MFB50 values were transferred in real-time to the ETAS ES910 RP device via CAN communication. The pressure-based control technique implemented on the ETAS device performs the  $SOI_{main}$  correction according to Eqs. (2-4), and sends the updated  $SOI_{main}$  values to the engine ECU for each injector via ETK communication, thus by-passing the standard  $SOI_{main}$  values derived from the engine maps. The RP device also receives additional variables from the ECU via ETK, such as the engine speed  $n$  and total injected quantity  $q_{f,inj}$ , which are needed by the control. These quantities are needed by the pressure-based control because the MFB50 target was mapped as a function of the engine load and speed conditions.

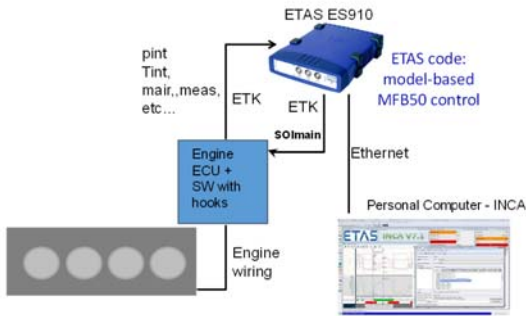
As far as the model-based technique setup is concerned (Fig. 6b), the ETAS RP device receives the needed input signals for the low-throughput heat release model from the ECU via ETK (see Fig. 3). The algorithm then evaluates the  $SOI_{main}$  value that allows the desired MFB50 target to be reached (see Fig. 3), and sends this value to the ECU via ETK, by-passing the standard values derived from the engine maps.

A modified version of the ECU software was needed in order to be able to by-pass the standard ECU function. Thus, several hooks were added to by-pass the variables (e.g.,  $SOI_{main}$ ).





(a): RP setup for testing the pressure-based technique



(b): RP setup for testing the model-based technique

Figure 6. Scheme of the RP setup for the pressure-based (a) and model-based (b) MFB50 control techniques.

## Results and discussion

### Model-in-the-loop

The pressure-based and model-based techniques were first developed and assessed by means of MiL.

As far as the pressure-based technique is concerned, the tests were mainly focused on obtaining an algorithm that could guarantee a stable and fast MFB50 control, especially in transient conditions.

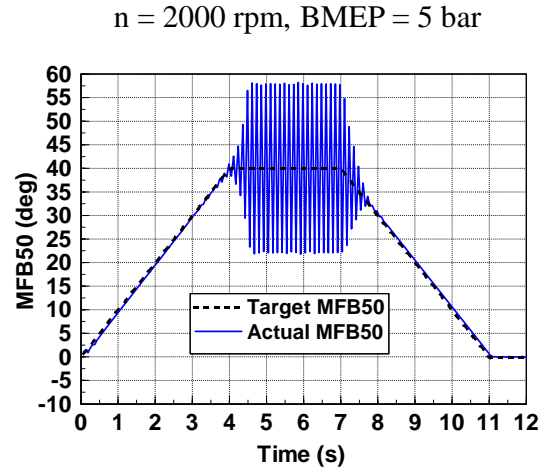
To this aim, several tests were carried out. The results shown in this section are related to simulations of MFB50 target ramps which were carried out at a fixed engine operating condition. First, a constant unitary value of the  $K_{m,i}^j$  coefficient used in Eq. (3) was set.

However, it was found that this assumption led to unstable operations.

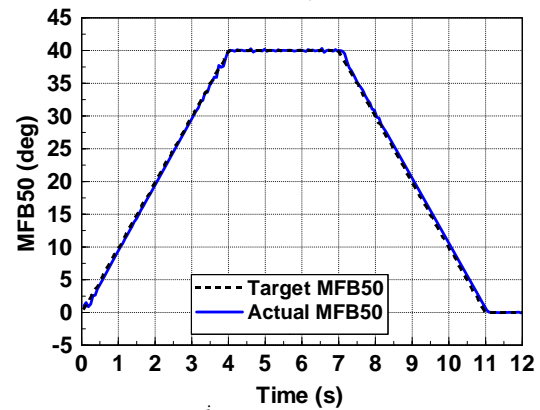
This can be seen in Fig. 7a, which reports the time histories of the MFB50 target (black dashed line) and the actual MFB50 (blue line), when the pressure-based technique was adopted and value of  $K_{m,i}^j$  equal to 1 was assumed in Eq. (3). The ramp was simulated at  $n=2000$  rpm and  $BMEP=5$  bar.

In order to avoid unstable behavior, the value of the  $K_{m,i}^j$  parameter was then varied cycle-by-cycle according to the strategy reported in Eq. (4). This strategy allows the correction of  $SOI_{main}$  to be reduced when the MFB50 error sign changes over two consecutive cycles (i.e., when the actual MFB50 value is close to the target one).

It can be noted in Fig. 7b that the instability was eliminated when this strategy was adopted.



(a):  $K_{m,i}^j = 1$

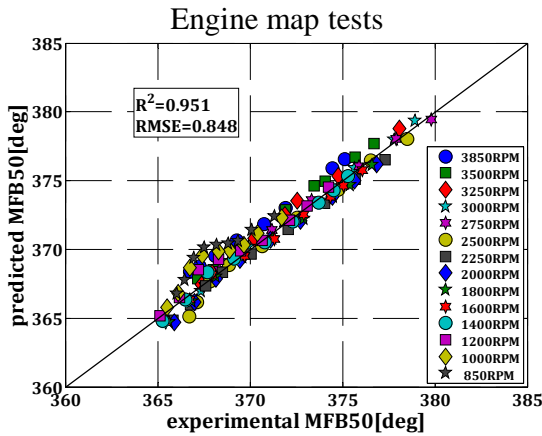


(b):  $K_{m,i}^j$  according to Eq. (4)

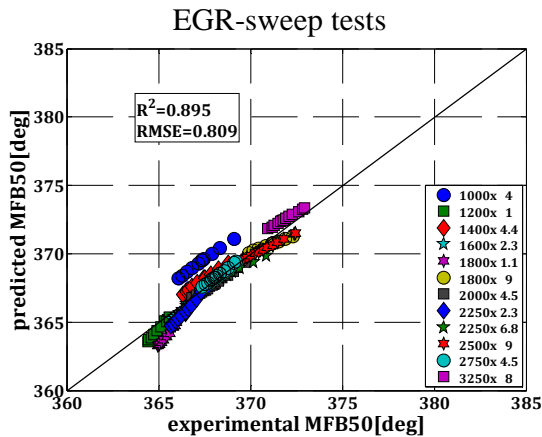
Figure 7. MiL: simulated trends of the target and actual MFB50, adopting different strategies for the definition of the  $K_{m,i}^j$  coefficient used in Eq. (3).

As far as the model-based MFB50 control technique is concerned, the low-throughput heat release model (see Eqs. (5-9)) was first calibrated over the steady-state tests shown in Fig. 2, and the correlations reported in Eqs. (10-14) were identified.

Figure 8 reports the predicted vs. experimental values of MFB50, obtained using the low-throughput heat release model for the engine-map tests (Fig. 8a) and EGR-sweep tests (Fig. 8b). The squared correlation coefficient  $R^2$  and the root mean square error (RMSE) are also reported in order to quantify the accuracy of the model.



(a)



(b)

Figure 8. Predicted vs. experimental values of MFB50 obtained with the low-throughput heat release model for the engine map tests (a) and EGR-sweep tests (b) reported in Fig. 2.

In general, it can be seen that the RMSE is of the order of 0.8 deg for both datasets, and the model is capable of predicting the effects of variations in the speed/load (Fig. 8a) and intake oxygen concentration at fixed operating condition on MFB50 (Fig. 8b). A slight deterioration in the MFB50 prediction accuracy can be noted for low-speed conditions (i.e.,  $n=1000\text{-}1200$  rpm). In order to reduce the error, the model was re-calibrated by splitting the dataset into different ranges, as a function of the engine speed, and identifying two separate correlation sets. However, this approach was found to lead to discontinuities of the control, especially in transient conditions, and in the end a single set of correlations was used (i.e., Eqs. (10-14)).

The model was then inverted according to the procedure shown in Fig. 3, and the resulting model-based control was implemented in Simulink and tested in MiL by means of the fast-running GT-power model, in order to check its functionality. It was verified that the number of required iterations ranges between 1 and 3, when the control is applied to the engine map tests. This also confirms the finding reported in [42]. As a result, a fixed number of three iterations was set for the model inversion.

## Hardware-in-the-loop

In the HiL phase, the developed controls were uploaded onto the ETAS ES910 RP device. ETAS Intecrio software was used to convert the Simulink code into the ETAS code. The RP device was then connected to the PXI device (used as a real-time engine emulator) via CAN communication (see Fig. 5), and both control techniques were tested in real-time.

The main objective of this phase was to check the real-time capability of both methods, with specific focus on the model-based technique, which requires a much higher computational effort than the pressure-based one. The ECU and the ETAS ES910 device exchange data every 180 crank angle degrees, and both controls must be able to run within that crank angle interval, otherwise a time overrun occurs. This crank angle interval corresponds to a period of 7.5 ms at 4000 rpm, which is the maximum engine speed and therefore represents the most restrictive operation interval for the controls.

The average computational time required by the controls, obtained by means of HiL, is shown in Tab. 4.

Table 4. HiL: average computational time required by the pressure-based and model-based techniques implemented in the ETAS ES910 RP device

	Average computational time on ETAS ES910 device
Pressure-based technique	~0.2 ms
Model-based technique (3 iterations, integration step of 0.1 deg)	~6 ms
Model-based technique (3 iterations, integration step of 0.2 deg)	~3 ms
Model-based technique (3 iterations, integration step of 1.0 deg)	~0.6 ms

As expected, the computational time required by the pressure-based technique was found to be much lower than the maximum available time of 7.5 ms.

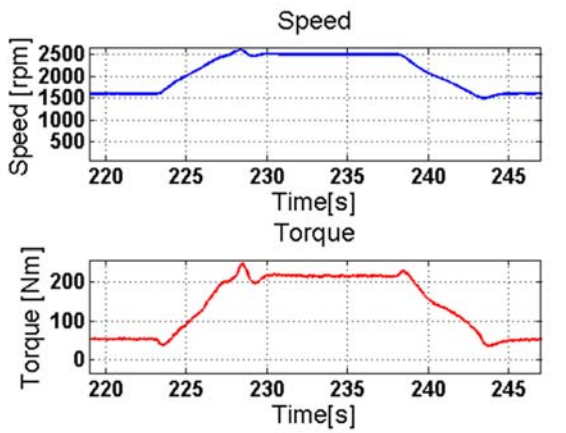
As far as the model-based technique is concerned, the required computational time was found to be a function of the number of iterations of the inverted model (see Fig. 3) and of the crank angle step used for the integration of the model equations. A fixed number of three iterations was set on the basis of the results obtained in the MiL phase. It can be seen in the table that the required computational time is a linear function of the adopted crank angle integration step. It was shown in [26] that the accuracy of the heat release model is not affected when the computational step is increased from 0.1 to 0.2 deg, and is still acceptable if a crank angle step of 1 deg is used.

An integration step of 0.2 deg was then adopted in the code implemented in the rapid prototyping device, in order to guarantee the maximum accuracy of the model.

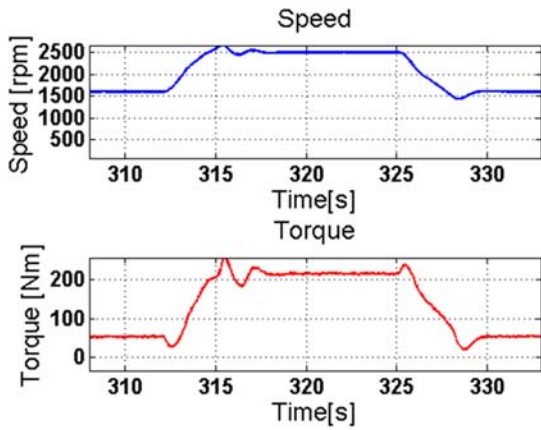
## Rapid prototyping

Finally, the developed control techniques were tested on the engine by connecting the ETAS ES910 device to the engine ECU via ETK communication (see Fig. 6). The results reported in this section are related to the testing of the controls over three transient tests, i.e., two speed/load ramps of different duration and a WHTC interval. Figure

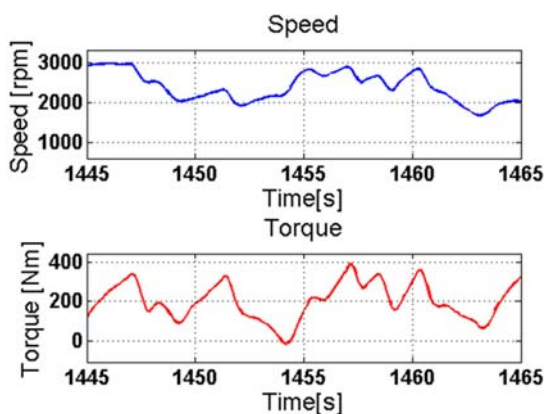
9 reports the time histories of the engine speed and torque for the three analyzed tests. The three transient tests were constituted by two speed/load ramps (n = 1600-2500 rpm, Torque = 55-215 Nm) of different duration, i.e., 5s (Fig. 9a, Test 1) and 3s (Fig. 9b, Test 2), and a WHTC interval (Fig. 9c, Test 3).



(a) Test 1: Torque/speed ramps (duration: 5s)



(b) Test 2: Torque/speed ramps (duration: 3s)



(c) Test 3: WHTC interval

Figure 9. Engine speed and torque as a function of time for the three analyzed transient tests.

It can be noted in Figs. 9b and 9b that some speed and load oscillations occur at the end of the ramps. These oscillations depend on the performance of the engine speed/load controllers implemented in the test bench automation system.

Each test was first performed without MFB50 control (the start of injection of the main pulse was actuated according to the ECU maps), and was then repeated adopting the pressure-based MFB50 control technique and the model-based MFB50 control technique.

The results related to the ‘Test1’, ‘Test2’ and ‘Test3’ cases are reported in Figs. 10-12, respectively.

The three charts in each figure report the MFB50 and  $SOI_{main}$  trends of each cylinder, for the baseline case in which the  $SOI_{main}$  values from engine maps are actuated (Figs. 10a, 11a, 12a), for the engine operation with the pressure-based MFB50 control (Figs. 10b, 11b, 12b) and for the engine operation with the model-based control (Figs. 10c, 11c, 12c).

The MFB50 target value is indicated in the figures with a black dashed line, and was calculated using a look-up table as a function of the engine speed and injected fuel quantity. This look-up table was built considering the measured values of MFB50 for the steady-state engine map tests reported in Fig. 2. The average value of the four cylinders was calculated for each operating condition and set as the target for that operating point. It should be noted that, in general, the optimal MFB50 target that has to be used in transient operation could be different from the steady-state value for a given engine speed/load condition. However, this aspect was not the focus of the present paper and will be investigated in the near future.

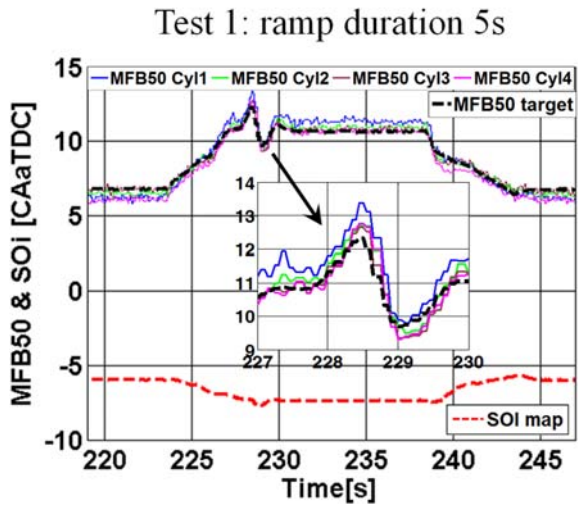
In all the figures, ‘SOImap’ (which is reported with a red dashed line) indicates the  $SOI_{main}$  value that is derived from the standard ECU maps, and which is actuated in the baseline case (i.e., Figs 10a, 11a, 12a). The trend of MFB50 target is also reported in the same figures as a reference, even though no MFB50 control was actuated in that case.

In general, it can be noted that the pressure-based technique (Figs. 10b, 11b, 11b) is very effective in reducing the cylinder-to-cylinder dispersion of MFB50, thanks to the individual control of  $SOI_{main}$ , and is capable of achieving the desired MFB50 target with limited overshooting/undershooting behavior.

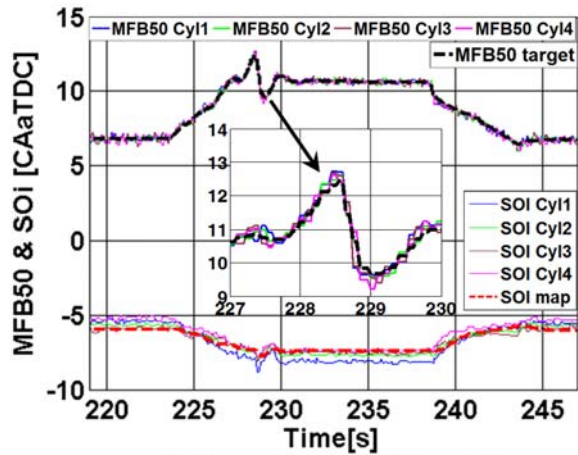
The adoption of the model-based control was found to provide very similar results to the baseline case. This means that the implemented combustion model is also effective in predicting the heat release in transient conditions.

It should be noted that the current version of the model-based control does not perform a cylinder-to-cylinder control of MFB50, because the input variables that have been used in the model (see Fig. 3) are not able to capture cylinder-to-cylinder MFB50 variations. However, the combustion model could be capable of predicting cylinder-to-cylinder combustion deviations due to effects which can be taken into account by the input variables (e.g., if the  $O_2$  concentration in each intake runner is provided as input, the model would be able to predict the effect of the non-homogenous distributions of EGR on MFB50).

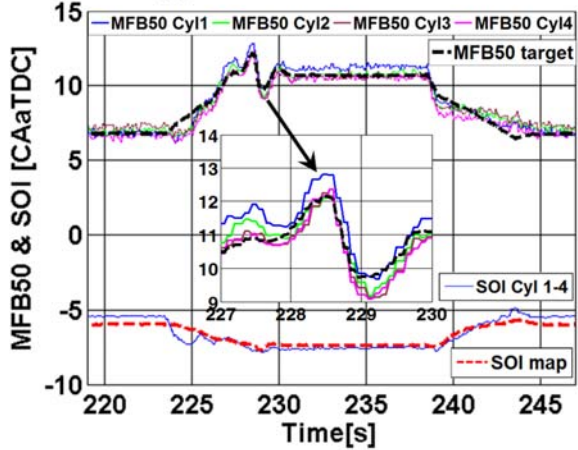




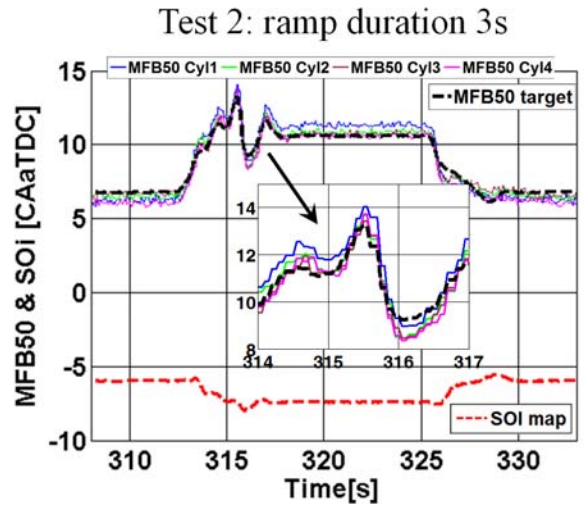
(a) Baseline case (SOI<sub>main</sub> from ECU maps).



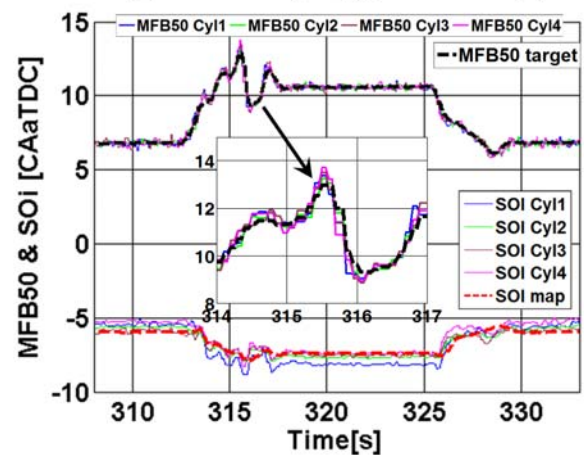
(b) Pressure-based MFB50 control



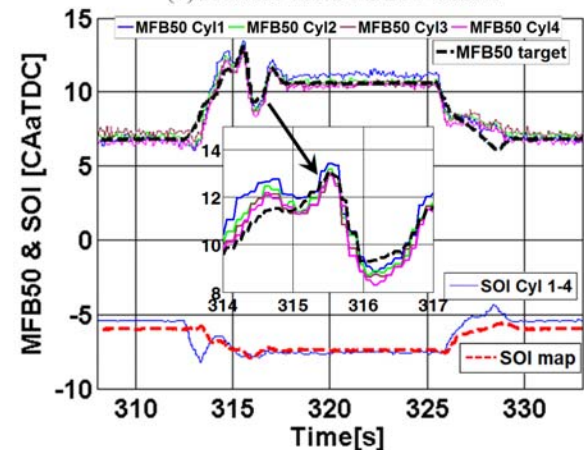
(c) Test 3: Model-based MFB50 control



(a) Baseline case (SOI<sub>main</sub> from ECU maps).



(b) Pressure-based MFB50 control

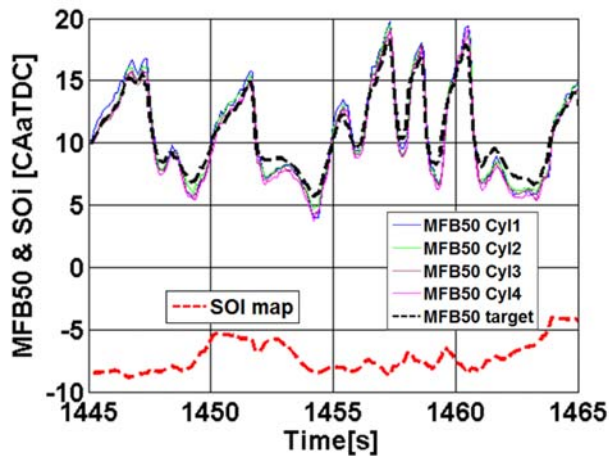


(c) Test 3: Model-based MFB50 control

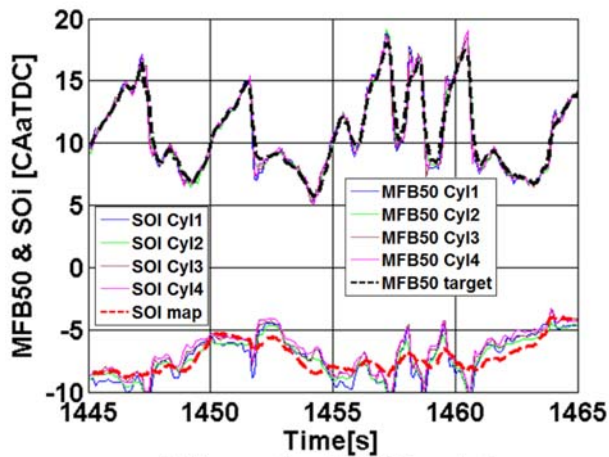
Figure 10. MFB50 and SOI<sub>main</sub> trends over the “Test 1” transient condition, for the baseline case (a), adopting the pressure-based MFB50 control (b) and adopting the model-based MFB50 control (c).

Figure 11. MFB50 and SOI<sub>main</sub> trends over the “Test 2” transient condition, for the baseline case (a), adopting the pressure-based MFB50 control (b) and adopting the model-based MFB50 control (c).

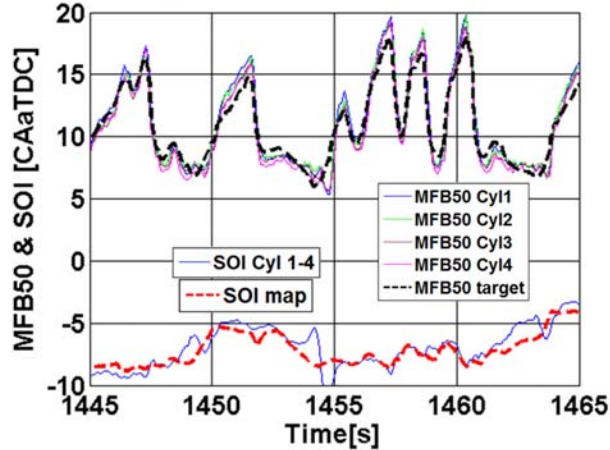
### Test 3: WHTC interval



(a) Baseline case (SOI<sub>main</sub> from ECU maps).



(b) Pressure-based MFB50 control



(c) Test 3: Model-based MFB50 control

Figure 12. MFB50 and SOI<sub>main</sub> trends over the ‘Test 3’ transient condition, for the baseline case (a), adopting the pressure-based MFB50 control (b) and adopting the model-based MFB50 control (c).

Table 5 reports the values of RMSE related to the deviations between the actual MFB50 of each cylinder and the target MFB50 for the three analyzed transient tests and for the three SOI actuation modes (baseline operation, pressure-based MFB50 control and model-based MFB50 control).

Table 5. RMSE values related to the deviations between the actual MFB50 values of each cylinder and the target MFB50.

RMSE (deg)	Cyl. 1	Cyl. 2	Cyl. 3	Cyl. 4
SOI <sub>main</sub> from engine maps	0.55	0.28	0.22	0.46
Pressure-based MFB50 control technique	0.17	0.14	0.18	0.16
Model-based MFB50 control technique	0.48	0.41	0.51	0.46

(a) Test 1

RMSE (deg)	Cyl. 1	Cyl. 2	Cyl. 3	Cyl. 4
SOI <sub>main</sub> from engine maps	0.63	0.36	0.29	0.52
Pressure-based MFB50 control technique	0.22	0.16	0.21	0.21
Model-based MFB50 control technique	0.59	0.48	0.56	0.48

(b) Test 2

RMSE (deg)	Cyl. 1	Cyl. 2	Cyl. 3	Cyl. 4
SOI <sub>main</sub> from engine maps	1.1	0.85	0.89	1.0
Pressure-based MFB50 control technique	0.74	0.45	0.72	0.65
Model-based MFB50 control technique	1.0	0.88	0.83	0.90

(c) Test 3

The RMSE values reported in the table for the MFB50 control techniques quantify the average deviation between the actual values of MFB50 measured in the cylinders and the target values. The MFB50 target was not used for the baseline case, because the ECU actuates the SOI<sub>main</sub> values that are derived from the engine maps. However, in this case, the RMSE quantifies the deviations between the MFB50 values measured in the cylinders over the transient tests, and the corresponding values at measured at steady-state conditions. It should be recalled that the MFB50 target was calculated using a look-up table as a function of the engine speed and injected fuel quantity. This look-up table was built considering the measured values of MFB50 for the steady-state engine map tests reported in Fig. 2.

The results reported in Tab. 5 confirm that the adoption of the pressure-based technique leads to the smallest deviation between the target and actual values of MFB50 and to an almost uniform behavior over all the cylinders, and that the performances of the baseline SOI actuation strategy and of the model-based technique are very similar to each other.

However, a great advantage of the model-based technique, compared to the baseline case, is that MFB50 can be set directly as a target. This in turn leads to several advantages. First, it should be noted that



MFB50 is more closely correlated to the combustion efficiency and to the in-cylinder pollutant formation than  $SOI_{main}$ . A model-based control is therefore robust to deviations in the engine parameters (e.g., intake T, p,  $O_2$  concentration, ...), with respect to the baseline dataset, as it is capable of predicting their effects on the combustion process (see Fig. 8). In order to take into account these effects, the baseline engine control requires a large number of correction maps, which must be calibrated on the basis of a costly and time-consuming experimental activity.

Moreover, a model-based approach is also expected to provide good control of the combustion phasing in transient operations, where large deviations of the engine parameters may occur with respect to the steady-state conditions (due, for example, to turbo-lag effects).

Finally, the model-based and pressure-based methods are expected to lead to advantages, especially for highly premixed combustion modes (such as PCCI), in which high EGR rates are employed in conjunction with early injection, which could lead to a significant deterioration in the combustion quality. An accurate MFB50 control could therefore be extremely important in this combustion mode in order to stabilize combustion.

## Future work

The results reported in the present paper are mainly related to the development and testing of pressure-based and model-based MFB50 control techniques in conventional combustion mode. However, the main goal of the research project is the investigation of the potential of PCCI combustion mode, which will be achieved by adopting high EGR levels in conjunction with early injection. To this aim, a new engine hardware specifically optimized for PCCI combustion has recently been at the test bench, and the test are currently ongoing. Preliminary tests have already been carried out in PCCI mode at low-load conditions for the conventional engine hardware. The results of these tests show that, in PCCI mode, the pressure-based method is effective in reducing the coefficient of variation of the peak firing pressure and of the indicated mean effective pressure, as well as the amplitude of the dispersion range of the combustion noise [43]. Moreover, a feed-forward controller with feedback correction will also be developed and tested. This controller will take into account both the measured MFB50 errors and the model-based MFB50 values.

## Summary/Conclusions

The present study has been devoted to the development of pressure-based and model-based techniques for the control of MFB50 (crank angle at which 50% of the fuel mass fraction has burned) on a 3.0L Euro VI diesel engine. The control techniques have been developed and assessed by means of Model-in-the-Loop (MiL) and Hardware-in-the-Loop (HiL) techniques, and have been tested on the engine using a rapid prototyping device. The experimental tests have been performed on a highly dynamic test bench at the Politecnico di Torino, in the frame of a joint research project with CNH/FPT Industrial, oriented toward the investigation of the potential of PCCI combustion.

The pressure-based technique requires the utilization of a pressure transducer for each cylinder, in order to diagnose the actual values of MFB50 cycle-by-cycle and cylinder-to-cylinder, and to perform a correction of the start of injection of the main pulse ( $SOI_{main}$ ) in order to achieve the desired MFB50 target, according to a closed-loop

approach. The model-based technique, instead, requires the adoption of a heat release predictive model that is capable of simulating MFB50. This control technique is based on heat release model inversion, in order to identify the optimal value of  $SOI_{main}$  that allows the desired MFB50 target to be achieved cycle-by-cycle. The approach is therefore of the open-loop type.

The control techniques have been developed and assessed in MiL and HiL. It has been verified that both methods are sufficiently fast to be executed on a rapid prototyping device (an ETAS ES910 in the present study) in order to achieve cycle-by-cycle and (for the pressure-based method) cylinder-to-cylinder MFB50 control. The methods have also been tested on the engine through rapid prototyping, over different speed/load ramps and over a WHTC interval.

These tests have shown that the pressure-based method is characterized by a very fast response and is effective in achieving the desired MFB50 target without any significant overshooting or undershooting behaviors. Moreover, this method is also capable of controlling the cylinder-to-cylinder MFB50 dispersion, as the pressure trace was measured in all of the cylinders.

It has been verified that the adoption of the model-based MFB50 control leads to a similar performance to that obtained when the standard  $SOI_{main}$  actuation based on engine maps is adopted. However, a great advantage of the model-based is that MFB50 can be set directly as a target for the control. This could lead to several advantages. MFB50 is in fact more closely correlated to the combustion efficiency and to the in-cylinder pollutant formation than  $SOI_{main}$ . A model-based control is therefore robust to deviations in the engine parameters (e.g., intake T, p,  $O_2$  concentration, ...), with respect to the nominal values, as it is capable of predicting their effects on the combustion process. In order to take into account these effects, the baseline engine control requires a large number of correction maps that must be calibrated on the basis of a costly and time-consuming experimental activity. Moreover, a model-based approach is also expected to provide good control of the combustion phasing in transient operations, where high deviations of the engine parameters may occur with respect to the steady-state conditions.

The two developed methods are also expected to lead to advantages in terms of combustion stabilization, for highly premixed combustion modes (such as PCCI), in which high EGR rates are employed in conjunction with early injection. This combustion mode may in fact lead to a deterioration in the combustion quality and to high cycle-by-cycle combustion variability. Tests on the PCCI combustion mode are currently underway and the results will be shown in the near future.

## References

1. Guido, C., Beatrice, C., Di Iorio, S., Napolitano, P. et al., "Assessment of Closed-Loop Combustion Control Capability for Biodiesel Blending Detection and Combustion Impact Mitigation for an Euro5 Automotive Diesel Engine," SAE Technical Paper 2011-01-1193, 2011, doi:[10.4271/2011-01-1193](https://doi.org/10.4271/2011-01-1193).
2. Saracino, R., Gaballo, M., Mannal, S., Motz, S. et al., "Cylinder Pressure-Based Closed Loop Combustion Control: A Valid Support to Fulfill Current and Future Requirements of Diesel Powertrain Systems," SAE Technical Paper 2015-24-2423, 2015, doi:[10.4271/2015-24-2423](https://doi.org/10.4271/2015-24-2423).

3. Chung, J., Oh, S., Min, K., and Sunwoo, M., "Real-time combustion parameter estimation algorithm for light-duty diesel engines using in-cylinder pressure measurement", *Applied Thermal Engineering* 60:33-43, 2013, doi:[10.4271/2009-01-1318](https://doi.org/10.4271/2009-01-1318).
4. Asad, U., and Zheng M., "Fast heat release characterization of a diesel engine", *International Journal of Thermal Sciences* 47:1688-1700, 2008, doi:[10.1016/j.ijthermalsci.2008.01.009](https://doi.org/10.1016/j.ijthermalsci.2008.01.009).
5. Catania, A., d'Ambrosio, S., Finesso, R., Spessa, E. et al., "Combustion System Optimization of a Low Compression-Ratio PCCI Diesel Engine for Light-Duty Application," *SAE Int. J. Engines* 2(1):1314-1326, 2009, doi:[10.4271/2009-01-1464](https://doi.org/10.4271/2009-01-1464).
6. Ponti, F., Ravaglioli, V., Moro, D., and Serra, G., "MFB50 on-board estimation methodology for combustion control", *Control Engineering Practice* 21(12):1821-1829, 2013, doi:[10.1016/j.conengprac.2013.05.001](https://doi.org/10.1016/j.conengprac.2013.05.001).
7. Ponti, F., Ravaglioli, V., Serra, G., and Stola, F., "Instantaneous engine speed measurement and processing for MFB50 evaluation", *SAE Int. J. Engines* 2(2):235-244, 2010, doi:[10.4271/2009-01-2747](https://doi.org/10.4271/2009-01-2747).
8. Ponti, F., Ravaglioli, V., Moro, D., and Serra, G., "Combustion control using a model-based MFB50 estimation methodology", Proceedings of the 6th IFAC symposium advances in automotive control, Munich, 2010, doi: [10.3182/20100712-3-DE-2013.00122](https://doi.org/10.3182/20100712-3-DE-2013.00122).
9. Finesso, R., and Spessa, E., "A Feed-Forward Approach for the Real-Time Estimation and Control of MFB50 and SOI In Diesel Engines," *SAE Int. J. Engines* 7(1):528-549, 2014, doi:[10.4271/2014-01-9046](https://doi.org/10.4271/2014-01-9046).
10. Reitz, R. D., and Rutland, C. J., "Development and testing of diesel engine CFD models" *Progress in Energy and Combustion Science* 21(2): 173-196, 1995, doi:[10.1016/0360-1285\(95\)00003-Z](https://doi.org/10.1016/0360-1285(95)00003-Z).
11. Cipolla, G., Vassallo, A., Catania, A., Spessa, E. et al., "Combined application of CFD modeling and pressure-based combustion diagnostics for the development of a low compression ratio high-performance diesel engine," SAE Technical Paper 2007-24-0034, 2007, doi:[10.4271/2007-24-0034](https://doi.org/10.4271/2007-24-0034).
12. Hiroyasu, H., "Diesel engine combustion and its modeling", Proceedings of the 1st International Symposium on Diagnostics and Modeling of Combustion in Internal Combustion Engines, Tokyo, Japan, 1985.
13. Hiroyasu, H., Kadota, T., and Arai, M., "Development and use of a spray combustion modeling to predict diesel engine efficiency and pollutant emissions: part 1 combustion modeling," *Bulletin of JSME*, vol. 26, pp. 569-575, 1983.
14. Jung, D. and Assanis, D., "Multi-Zone DI Diesel Spray Combustion Model for Cycle Simulation Studies of Engine Performance and Emissions," SAE Technical Paper 2001-01-1246, 2001, doi:[10.4271/2001-01-1246](https://doi.org/10.4271/2001-01-1246).
15. Ponti, F., Corti, E., Serra, G., and De Cesare, M., "Common Rail Multi-Jet Diesel Engine Combustion Model Development for Control Purposes", SAE Technical Paper 2007-01-0383, 2007, doi:[10.4271/2007-01-0383](https://doi.org/10.4271/2007-01-0383).
16. Ponti, F., Ravaglioli, V., Moro, D., and Serra, G., "MFB50 On-Board Evaluation Based on a Zero-Dimensional ROHR Model", SAE Technical Paper 2011-01-1420, 2011, doi:[10.4271/2011-01-1420](https://doi.org/10.4271/2011-01-1420).
17. Arrègle, J., García, J.M., López, J.J., Fenollosa, C., "Development of a zero-dimensional Diesel combustion model. Part 1: Analysis of the quasi-steady diffusion combustion phase", *Applied Thermal Engineering* 23(11):1301-1317, 2003, doi:[10.1016/S1359-4311\(03\)00079-6](https://doi.org/10.1016/S1359-4311(03)00079-6).
18. Arrègle, J., García, J.M., López, J.J., Fenollosa, C., "Development of a zero-dimensional Diesel combustion model. Part 2: Analysis of the transient initial and final diffusion combustion phases", *Applied Thermal Engineering* 23(11):1319-1331, 2003, doi:[10.1016/S1359-4311\(03\)00080-2](https://doi.org/10.1016/S1359-4311(03)00080-2).
19. Chmela, F.G., and Orthaber, G.C., "Rate of Heat Release Prediction for Direct Injection Diesel Engines Based on Purely Mixing Controlled Combustion", SAE Technical Paper 1999-01-0186, 1999, doi:[10.4271/1999-01-0186](https://doi.org/10.4271/1999-01-0186).
20. Egnell, R., "A Simple Approach to Studying the Relation between Fuel Rate, Heat Release Rate and NO Formation in Diesel Engines", SAE Technical Paper 1999-01-3548, 1999, doi:[10.4271/1999-01-3548](https://doi.org/10.4271/1999-01-3548).
21. Ryan, T. W., and Callahan, T.J., "Homogeneous Charge Compression Ignition of Diesel Fuels". SAE Technical Paper 961160, 1996, doi:[10.4271/961160](https://doi.org/10.4271/961160).
22. Ericson, C., Westerberg, B., Andersson, M., and Egnell, R., "Modelling Diesel Engine Combustion and NOx Formation for Model Based Control and Simulation of Engine and Exhaust Aftertreatment Systems", SAE Technical Paper 2006-01-0687, 2006, doi:[10.4271/2006-01-0687](https://doi.org/10.4271/2006-01-0687).
23. Grahn, M., Olsson, J.O., and McKelvey, T., "A Diesel Engine Model for Dynamic Drive Cycle Simulations", 18th IFAC World Congress Milano (Italy) August 28 - September 2, 2011, doi:[10.3182/20110828-6-IT-1002.03541](https://doi.org/10.3182/20110828-6-IT-1002.03541).
24. Tazua, X., Maiboom, A., Chesse, P., and Thouvenel, N., "A new phenomenological heat release model for thermodynamical simulation of modern turbocharged heavy duty Diesel engines", *Applied Thermal Engineering* 26:1851-1857, 2006, doi:[10.1016/j.applthermaleng.2006.02.009](https://doi.org/10.1016/j.applthermaleng.2006.02.009).
25. Catania, A.E., Finesso, R., and Spessa, E., "Predictive Zero-Dimensional Combustion Model for DI Diesel Engine Feed-Forward Control", *Energy Conversion and Management* 52(10):3159-3175, 2011, doi:[10.1016/j.enconman.2011.05.003](https://doi.org/10.1016/j.enconman.2011.05.003).
26. Finesso, R., Spessa, E., Yang, Y., Alfieri, V. et al., "HRR and MFB50 Estimation in a Euro 6 Diesel Engine by Means of Control-Oriented Predictive Models," *SAE Int. J. Engines* 8(3):1055-1068, 2015, doi:[10.4271/2015-01-0879](https://doi.org/10.4271/2015-01-0879).
27. Baratta, M., Finesso, R., Misul, D., and Spessa, E., "Comparison between Internal and External EGR Performance on a Heavy Duty Diesel Engine by Means of a Refined 1D Fluid-Dynamic Engine Model," *SAE Int. J. Engines* 8(5):1977-1992, 2015, doi:[10.4271/2015-24-2389](https://doi.org/10.4271/2015-24-2389).
28. Hennings Och, S., Moura, L.M., Cocco Mariani, V., Coelho, L.S., et al., "Volumetric efficiency optimization of a single-cylinder D.I. diesel engine using differential evolution algorithm", *Applied thermal engineering* 108:660-669, 2016, doi:[10.1016/j.applthermaleng.2016.07.042](https://doi.org/10.1016/j.applthermaleng.2016.07.042).
29. Liu, B., Zhao, C., Zhang, F., Cui, T., et al., "Misfire detection of a turbocharged diesel engine by using artificial neural networks", *Applied thermal engineering* 55(1-2):26-32, 2013, doi: [10.1016/j.applthermaleng.2013.02.032](https://doi.org/10.1016/j.applthermaleng.2013.02.032).
30. Saraswati, S., Agarwal, P.K., and Chand, S., "Neural networks and fuzzy logic-based spark advance control of SI engines", *Expert Systems with Applications* 38(6):6916-6925, 2011, doi: [10.1016/j.eswa.2010.12.032](https://doi.org/10.1016/j.eswa.2010.12.032).
31. Barakat, M. and Abdelaziz, M., "Neural Network Transmission Control," SAE Technical Paper 2016-01-0089, 2016, doi:[10.4271/2016-01-0089](https://doi.org/10.4271/2016-01-0089).
32. Uzun, A., "Air mass flow estimation of diesel engines using neural network", *Fuel* 117(Part A):833-838, 2014, doi: [10.1016/j.fuel.2013.09.078](https://doi.org/10.1016/j.fuel.2013.09.078).
33. Sardarmehni, T., Keighobadi, J., Menhaj, M.B., and Rahmani, H., "Robust predictive control of lambda in internal combustion engines using neural networks", *Archives of Civil and*

- Mechanical Engineering* 13(4):432-443, 2013, doi: [10.1016/j.acme.2013.05.003](https://doi.org/10.1016/j.acme.2013.05.003).
34. Asik, J., Peters, J., Meyer, G., and Tang, D., "Transient A/F Estimation and Control Using a Neural Network," SAE Technical Paper 970619, 1997, doi:[10.4271/970619](https://doi.org/10.4271/970619).
  35. Yap, W.K., Ho, T., and Karri, V., "Exhaust emissions control and engine parameters optimization using artificial neural network virtual sensors for a hydrogen-powered vehicle", *International Journal of Hydrogen Energy* 37(10):8704-8715, 2012, doi: [10.1016/j.ijhydene.2012.02.153](https://doi.org/10.1016/j.ijhydene.2012.02.153).
  36. Uzun, A., "A parametric study for specific fuel consumption of an intercooled diesel engine using a neural network", *Fuel* 93:189-199, 2012, doi: [10.1016/j.fuel.2011.11.004](https://doi.org/10.1016/j.fuel.2011.11.004).
  37. Bennett, C., Dunne, J.F., Trimby, S., and Richardson, D., "Engine cylinder pressure reconstruction using crank kinematics and recurrently-trained neural networks", *Mechanical Systems and Signal Processing* 85:126-145, 2016, doi: [10.1016/j.ymsp.2016.07.015](https://doi.org/10.1016/j.ymsp.2016.07.015).
  38. Janakiraman, V.M., Nguyen, X., and Assanis, D., "Nonlinear identification of a gasoline HCCI engine using neural networks coupled with principal component analysis", *Applied Soft Computing* 13(5):2375-2389, 2013, doi: [10.1016/j.asoc.2013.01.006](https://doi.org/10.1016/j.asoc.2013.01.006).
  39. Heywood, J.B., "Internal Combustion Engine Fundamentals", McGraw-Hill Intern. Editions, 1988.
  40. Finesso, R., and Spessa, E., "Ignition delay prediction of multiple injections in diesel engines", *Fuel* 119(1):170-190, 2014, doi: [10.1016/j.fuel.2013.11.040](https://doi.org/10.1016/j.fuel.2013.11.040).
  41. Finesso, R., Spessa, E., and Yang, Y., "Development and Validation of a Real-Time Model for the Simulation of the Heat Release Rate, In-Cylinder Pressure and Pollutant Emissions in Diesel Engines," *SAE Int. J. Engines* 9(1):322-341, 2016, doi:[10.4271/2015-01-9044](https://doi.org/10.4271/2015-01-9044).
  42. Finesso R., Spessa E., and Yang, Y., "Fast estimation of combustion metrics in DI Diesel Engines for control-oriented applications", *Energy Conversion and Management* 112:254-273, 2016, doi:[10.1016/j.enconman.2016.01.018](https://doi.org/10.1016/j.enconman.2016.01.018).
  43. D'Ambrosio S., Hardy G., Iemmolo D., Mancarella A. et al., "Steady-State and Transient Operations of a Euro VI 3.0L HD Diesel Engine with Innovative Model-Based and Pressure-Based Combustion Control Techniques", SAE Technical paper 2017-01-0695, 2017, doi:[10.4271/2017-01-0695](https://doi.org/10.4271/2017-01-0695).

## Contact Information

Ezio Spessa (Associate Professor)

IC Engines Advanced Laboratory

Dipartimento Energia, Politecnico di Torino

c.so Duca degli Abruzzi, 24 - 10129 Torino (Italy)

phone: +39-011-090.4482

ezio.spessa@polito.it.

## Definitions/Abbreviations

**ANN** Artificial neural network

<b>BMEP</b>	Brake Mean Effective Pressure
<b>CA</b>	crank angle
$c_p$	specific heat at constant pressure
$c_v$	specific heat at constant volume
<b>ECU</b>	Engine Control Unit
<b>EGR</b>	Exhaust Gas Recirculation
<b>FPT</b>	Fiat Powertrain Technologies
<b>GA</b>	Genetic algorithm
<b>HL</b>	lower heating value of the fuel
<b>HiL</b>	Hardware-in-the-Loop
<b>HRR</b>	Heat Release Rate
<b>IMEP</b>	Indicated Mean Effective Pressure
<b>K</b>	combustion rate coefficient
$K_{m,i}^j$	modulation factor of the pressure-based MFB50 control
<b>m</b>	mass
$\dot{m}_{f,inj}$	fuel injection rate
<b>m<sub>air,meas</sub></b>	measured trapped air mass
<b>m<sub>EGR</sub></b>	trapped mass of EGR
<b>m<sub>ind</sub></b>	total inducted mass
<b>MAF</b>	mass air flow sensor
<b>MFB50</b>	crank angle at which 50% of the fuel mass fraction has burned
<b>MiL</b>	Model-in-the-Loop
<b>n</b>	engine rotational speed
<b>NCD</b>	nozzle closure delay
<b>NOD</b>	nozzle opening delay

<b>O<sub>2</sub></b>	intake charge oxygen concentration	<b>RP</b>	Rapid Prototyping
<b>p</b>	pressure	<b>SOC</b>	start of combustion
<b>p<sub>f</sub></b>	injection pressure	<b>SOI</b>	electric start of Injection
<b>PCCI</b>	Premixed Charge Compression Ignition	<b>SOI<sub>main</sub></b>	Electric start of injection of the main pulse
<b>PFP</b>	Peak firing pressure	<b>SVM</b>	Support vector machine
<b>PXI</b>	PCI eXtensions for Instrumentation	<b>t</b>	time
<b>p<sub>int</sub></b>	intake manifold pressure	<b>T</b>	temperature
<b>pil</b>	pilot injection	<b>T<sub>int</sub></b>	intake manifold temperature
<b>q</b>	injected fuel volume quantity	<b>V</b>	in-cylinder volume
<b>Q<sub>ch</sub></b>	chemical heat release	<b>VGT</b>	Variable Geometry Turbocharger
<b>Q<sub>fuel</sub></b>	chemical energy associated with the injected fuel	<b>WHTC</b>	World Harmonized Transient Cycle
<b>Q<sub>net</sub></b>	net energy of the charge	<b>X<sub>r</sub></b>	EGR rate
<b>q<sub>f,inj</sub></b>	total injected fuel volume quantity	<b><i>Greek symbols</i></b>	
<b>q<sub>main</sub></b>	injected fuel volume quantity of the main injection	$\gamma = c_p/c_v$	specific heat ratio
<b>q<sub>pil</sub></b>	injected fuel volume quantity of the pilot injection	$\lambda$	relative air-to-fuel ratio
<b>q<sub>pil,tot</sub></b>	total injected fuel volume quantity of the pilot injections	$\rho$	density
<b>R<sup>2</sup></b>	squared correlation coefficient	$\rho_{SOI}$	in-chamber ambient density evaluated at the SOI instant
<b>RMSE</b>	root mean square error	$\rho_{SOC}$	in-chamber ambient density evaluated at the SOC instant
		$\tau$	ignition delay coefficient

## Appendix

### Comparison between the detailed and fast-running GT-power models

The fast-running model was developed by means of a simplification of a detailed GT-power engine model, which is shown in Fig. A1.

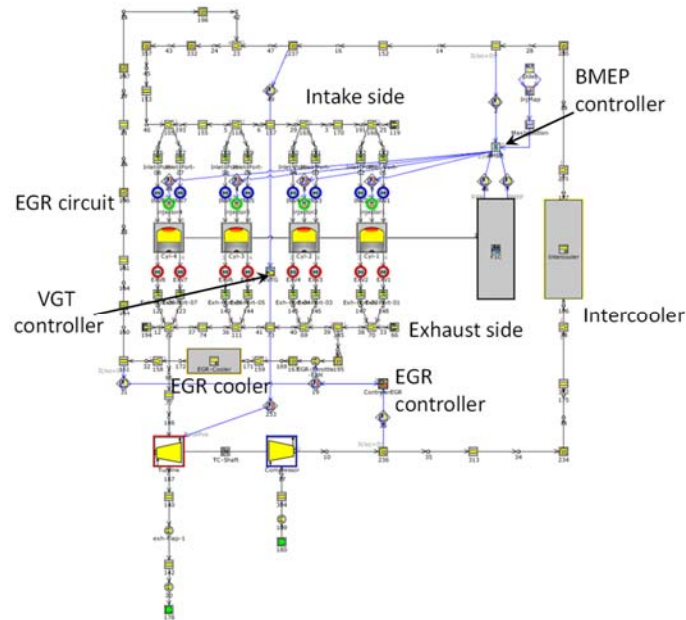
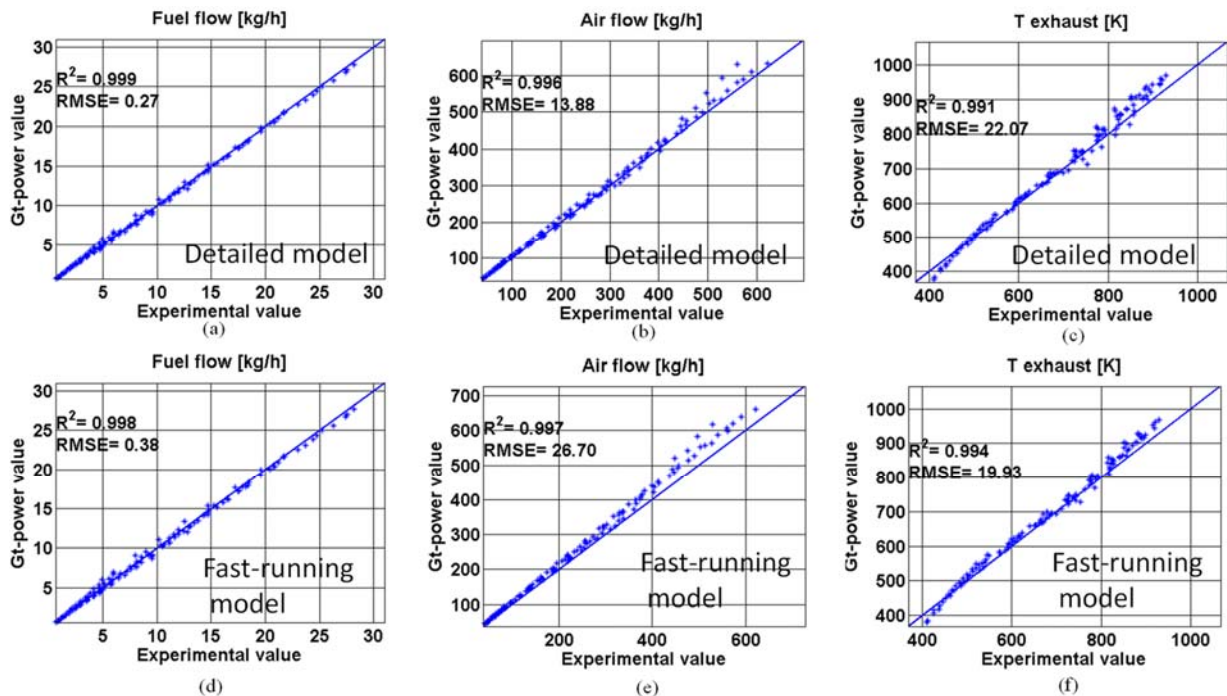


Figure A1. Scheme of the detailed GT-power model.

The performance of the detailed and fast-running models was compared against experimental data for the engine map tests reported in Fig. 2, and the results are shown in Figs. A2-A3.



re

Figure A2. Predicted vs. experimental values of the fuel flow, air flow and exhaust temperature for the detailed (a, b, c) and fast-running (d, e, f) GT-power models, for the engine map tests reported in Fig. 2.



Figure A2 reports a comparison (along with the values of  $R^2$  and RMSE) between the two models in terms of prediction of fuel mass flow rate, air mass flow rate and exhaust gas temperatures, while Fig. A3 reports a comparison in terms of in-cylinder combustion metrics (i.e., Peak Firing Pressure and MFB50). It can be seen that the performance of the two models is very similar, even though the real-time factor of the fast-running model is much shorter than that of the detailed model (0.9 vs. 20).

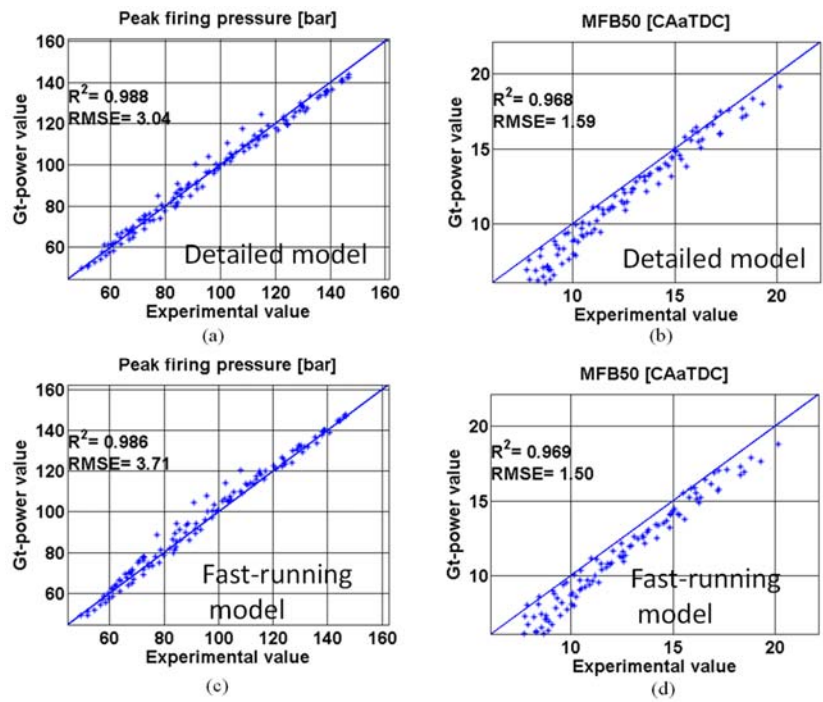


Figure A3. Predicted vs. experimental values of the peak firing pressure and MFB50 for the detailed (a, b) and fast-running (c, d) GT-power models, for the engine map tests reported in Fig. 2.